Thermoelectric effects in transport through quantum dots attached to ferromagnetic leads with noncollinear magnetic moments

R. Świrkowicz,[1] M. Wierzbicki,[1] and J. Barnaś[2,3]
[1]*Faculty of Physics, Warsaw University of Technology, ul. Koszykowa 75, 00-662 Warsaw, Poland*
[2]*Department of Physics, Adam Mickiewicz University, ul. Umultowska 85, 61-614 Poznań, Poland*
[3]*Institute of Molecular Physics, Polish Academy of Sciences, ul. Smoluchowskiego 17, 60-179 Poznań, Poland*
(Received 29 July 2009; revised manuscript received 10 October 2009; published 6 November 2009)

Charge transport accompanied by heat transfer through a single-level quantum dot coupled to ferromagnetic leads with noncollinear magnetic moments is studied theoretically in the linear and nonlinear transport regimes. Calculations performed in the framework of nonequilibrium Green's function formalism and the equation of motion method reveal a significant influence of Coulomb blockade on thermal transport processes. The thermopower S and thermal efficiency described by the figure of merit ZT depend on magnetic configuration of the system. Two physically different situations are considered; one appears when spin accumulation is excluded and the second one when spin accumulation is relevant. In the latter case we also calculate the corresponding spin thermopower. Apart from this, magnetothermopower is introduced and discussed.

DOI: 10.1103/PhysRevB.80.195409 PACS number(s): 73.23.Hk, 73.50.Lw, 85.80.Fi

I. INTRODUCTION

Electronic transport in nanostructures has been extensively studied in the last two decades. Recently, there is additionally a great interest in the charge transport accompanied by the energy (heat) transfer.[1–14] This applies to nanostructures of various types, including also quantum dots, on which we focus in this paper. Thermopower, quantitatively described by the Seebeck coefficient S and defined as the ratio of the voltage drop ΔV generated by the temperature difference ΔT, $S=\Delta V/\Delta T$, has been investigated experimentally and theoretically for quantum dots and molecules in the Coulomb blockade[15–21] and Kondo regimes.[22–27] Though applications of the thermal effects in nanoelectronic devices is still a matter of perspectives, the research of novel transport phenomena is of fundamental interest. Due to level quantization and Coulomb blockade effects, the situation in nanoscopic systems is different from that in bulk materials. Both charging energy and quantum confinement have been shown to strongly affect thermoelectric properties. Some novel effects such as oscillations of the thermopower S (Refs. 15 and 16) and oscillations of the thermal conductance κ (Refs. 20, 21, and 28) with the gate voltage have been observed in transport through Coulomb islands. Apart from this, additional fine structure due to discrete levels was found for small quantum dots (QDs).[17] Moreover, thermopower also appears to be a very sensitive tool to detect the Kondo correlations which lead to logarithmic dependence of the thermoelectric coefficients on temperature and also to sign reversal of S.[22] It is also worth noting that experiments performed on QDs in the Kondo regime reveal a strong influence of spin correlations on the thermopower.[26]

Coulomb interactions in QD-based single-electron devices have a significant influence on thermoelectric transport coefficients, and lead to strong violation of the Wiedeman-Franz law.[20,28] The Lorentz ratio, $L=\kappa/GT$, with G denoting the electric conductance and T standing for temperature, strongly depends on the gate voltage and can be significantly different from the Lorentz number $\pi k^2/3e^2$ typical for bulk systems, where k is the Boltzmann constant and e stands for the electron charge. Violation of the Wiedeman-Franz law was also observed for QDs in the Kondo regime.[24] As shown by Murphy *et al.*,[29] violation of the Wiedeman-Franz law is the main mechanism of an enhanced thermoelectric efficiency in molecular junctions, which can be important for possible applications in energy conversion devices. Additional advantage of molecular systems is that the corresponding phonon contributions to thermal conductance may be small.[1,30] Moreover, a giant thermopower was found in single-molecular systems.[30] Calculations based on the density-functional formalism indicate that the thermoelectric efficiency of molecules which exhibit the Fano resonance can be significantly enhanced. It is also worth to note, that the influence of the Kondo effect and quantum interference on thermoelectric properties in a QD side coupled to a quantum wire was studied by Yoshida *et al.*[27] in terms of the numerical renormalization group.

There is currently an increasing interest in the interplay of spin effects and heat transport. The spin Seebeck effect has been observed experimentally,[31] where also spin voltage generated by a temperature gradient in metallic magnets has been measured. It is expected that this effect may find applications in magnetoelectronic devices as a source of spin current. We also note, that the giant magnetothermoelectric power was observed in multilayered nanopillars,[32] while thermally excited spin currents were investigated in metals with embedded ferromagnetic clusters.[33,34] Quite recently, Hatami *et al.*[35] have studied Peltier and Seebeck effects in magnetic multilayers within the finite-element theory. They showed that thermoelectric effects significantly depend on relative alignment of magnetizations in neighboring magnetic layers. Thermoelectric effects in a single-level QD coupled to ferromagnetic leads have been discussed recently by Dubi and Di Ventra[36] in the sequential tunneling regime in terms of the rate equations.

Here, we present the approach to spin-dependent thermoelectric phenomena in transport through QDs using the nonequilibrium Green's function formalism. We study the sys-

tem composed of a QD attached to ferromagnetic leads with noncollinear magnetic moments and consider the interplay of magnetic and thermoelectric properties in the Coulomb (and quantum) blockade regime. First, in Secs. II and III we describe the basic thermoelectric effects and the model of a quantum dot coupled to external ferromagnetic leads, respectively. In Sec. IV we present the corresponding numerical results. Then, in Sec. V we introduce spin thermopower. Nonlinear thermopower is briefly discussed in Sec. VI. Final conclusions and summary are in Sec. VII.

II. THERMOELECTRIC PHENOMENA

The system to be considered consists of a small (single-level) QD attached to external ferromagnetic electrodes. The leads in equilibrium are described by the chemical potential μ and temperature T. We assume now that the chemical potential in nonequilibrium situation (in a biased system) is independent of electron spin. Though the spin dependence of tunneling processes through the dot may generally lead to spin accumulation (spin splitting of the chemical potential) in the electrodes, we assume the size of the electrodes is sufficiently large and spin-relaxation time sufficiently short to neglect this effect. In Sec. V, however, we will relax this assumption.

Let us now recall some basic formulas describing thermoelectric effects. Assume voltage ΔV and temperature difference ΔT between the two leads. The linear response theory gives then the following formulas for the charge current I and heat (energy) current I_Q flowing through the system:[37]

$$I = eL_0\Delta\mu + \frac{e}{T}L_1\Delta T, \tag{1}$$

$$I_Q = -L_1\Delta\mu - \frac{1}{T}L_2\Delta T \tag{2}$$

with $\Delta\mu = e\Delta V$. Here, L_n $(n=0,1,2)$ are defined as

$$L_n = -\frac{1}{\hbar}\mathrm{Tr}\int \frac{dE}{2\pi}(E-\mu)^n\mathbf{T}(E)\frac{\partial f}{\partial E}, \tag{3}$$

where $f(E)$ is the Fermi-Dirac distribution function, and $\mathbf{T}(E)$ describes transmission probability through the dot. The latter quantity is a matrix in the spin space.

The thermopower S is usually calculated as the voltage drop induced by the temperature difference under the condition that the charge current vanishes, $I=0$. This leads to the following well-known formula for S:

$$S = \frac{\Delta V}{\Delta T} = -\frac{1}{eT}\frac{L_1}{L_0}. \tag{4}$$

From Eqs. (1) and (2) follows that the electrical conductance G and thermal conductance κ are given by:[37]

$$G = e^2L_0 \tag{5}$$

and

$$\kappa = \frac{1}{T}\left(L_2 - \frac{L_1^2}{L_0}\right). \tag{6}$$

In turn, the thermoelectric efficiency of the system is described by the dimensionless figure of merit,

$$ZT = \frac{GS^2T}{\kappa}, \tag{7}$$

defined in terms of measurable coefficients S, G, and κ. To calculate these coefficients one needs to find the transmission matrix $\mathbf{T}(E)$, which includes the relevant information on transport properties of the system considered. Therefore, we calculate now $\mathbf{T}(E)$ for a QD attached to ferromagnetic leads.

III. MODEL OF A QUANTUM DOT COUPLED TO EXTERNAL FERROMAGNETIC LEADS

A quantum dot coupled to ferromagnetic leads can be described by Hamiltonian of the general form, $H=H_D+H_e+H_T$. The term H_D corresponds to the single-level dot and takes the form

$$H_D = \sum_\sigma \varepsilon_0 d_\sigma^+ d_\sigma + U d_\uparrow^+ d_\uparrow d_\downarrow^+ d_\downarrow, \tag{8}$$

where ε_0 is the dot energy level, and $d_\sigma^+(d_\sigma)$ is the creation (annihilation) operator of an electron with spin $\sigma=\uparrow(\downarrow)$. The intradot Coulomb interaction is described by the last term in H_D, with U denoting the Hubbard parameter. The second term in H is the lead Hamiltonian, $H_e = \sum_{\beta=L,R}\sum_{\mathbf{k}s}\varepsilon_{\mathbf{k}\beta s}c_{\mathbf{k}\beta s}^+ c_{\mathbf{k}\beta s}$, which describes noninteracting electrons with the wave vectors $\mathbf{k}$ and spin $s=+(-)$ in the left (L) and right (R) electrodes. We remind that the spin orientation in the dot's (global) quantization system is denoted by $\sigma=\uparrow(\downarrow)$, while in the local reference frames (determined by local magnetization orientation) of the leads as $s=+(-)$ for spin-majority (spin-minority) electrons. The last term in Hamiltonian H, $H_T = \sum_{\mathbf{k}\beta}\sum_{s\sigma}(V_{\mathbf{k}\beta}^{s\sigma}c_{\mathbf{k}\beta s}^+ d_\sigma + \mathrm{H.c.})$, describes tunneling processes between the dot and leads, with

$$\mathbf{V}_{\mathbf{k}L} = \begin{pmatrix} T_{\mathbf{k}L}^+ & 0 \\ 0 & T_{\mathbf{k}L}^- \end{pmatrix}, \quad \mathbf{V}_{\mathbf{k}R} = \begin{pmatrix} T_{\mathbf{k}R}^+\cos(\theta/2) & T_{\mathbf{k}R}^+\sin(\theta/2) \\ -T_{\mathbf{k}R}^-\sin(\theta/2) & T_{\mathbf{k}R}^-\cos(\theta/2) \end{pmatrix}. \tag{9}$$

Here, θ is the angle between magnetic moments of the two leads, and for the quantum dot we assumed the same quantization axis as in the left electrode.[38]

In the following, coupling of the dot to external leads will be described by the parameters expressed in the matrix form as:

$$\mathbf{\Gamma}^L = \begin{pmatrix} \Gamma_\uparrow^L & 0 \\ 0 & \Gamma_\downarrow^L \end{pmatrix}, \quad \mathbf{\Gamma}^R = \begin{pmatrix} \Gamma_\uparrow^R & \Gamma_{\uparrow\downarrow}^R \\ \Gamma_{\downarrow\uparrow}^R & \Gamma_\downarrow^R \end{pmatrix}, \tag{10}$$

where the following notation has been introduced: $\Gamma_\uparrow^L=\Gamma_+^L$, $\Gamma_\downarrow^L=\Gamma_-^L$, $\Gamma_\uparrow^R=\Gamma_+^R\cos^2(\theta/2)+\Gamma_-^R\sin^2(\theta/2)$, $\Gamma_\downarrow^R=\Gamma_+^R\sin^2(\theta/2)+\Gamma_-^R\cos^2(\theta/2)$, and $\Gamma_{\uparrow\downarrow}^R=\Gamma_{\downarrow\uparrow}^R=\frac{1}{2}(\Gamma_+^R-\Gamma_-^R)\sin\theta$. Here, $\Gamma_s^\beta=\Sigma_{\mathbf{k}}|T_{\mathbf{k}\beta}^s|^2\delta(E-\varepsilon_{\mathbf{k}\beta s})$, and we write Γ_s^β in the form $\Gamma_s^\beta=\Gamma(1+sp)$, where Γ is treated as a parameter independent of

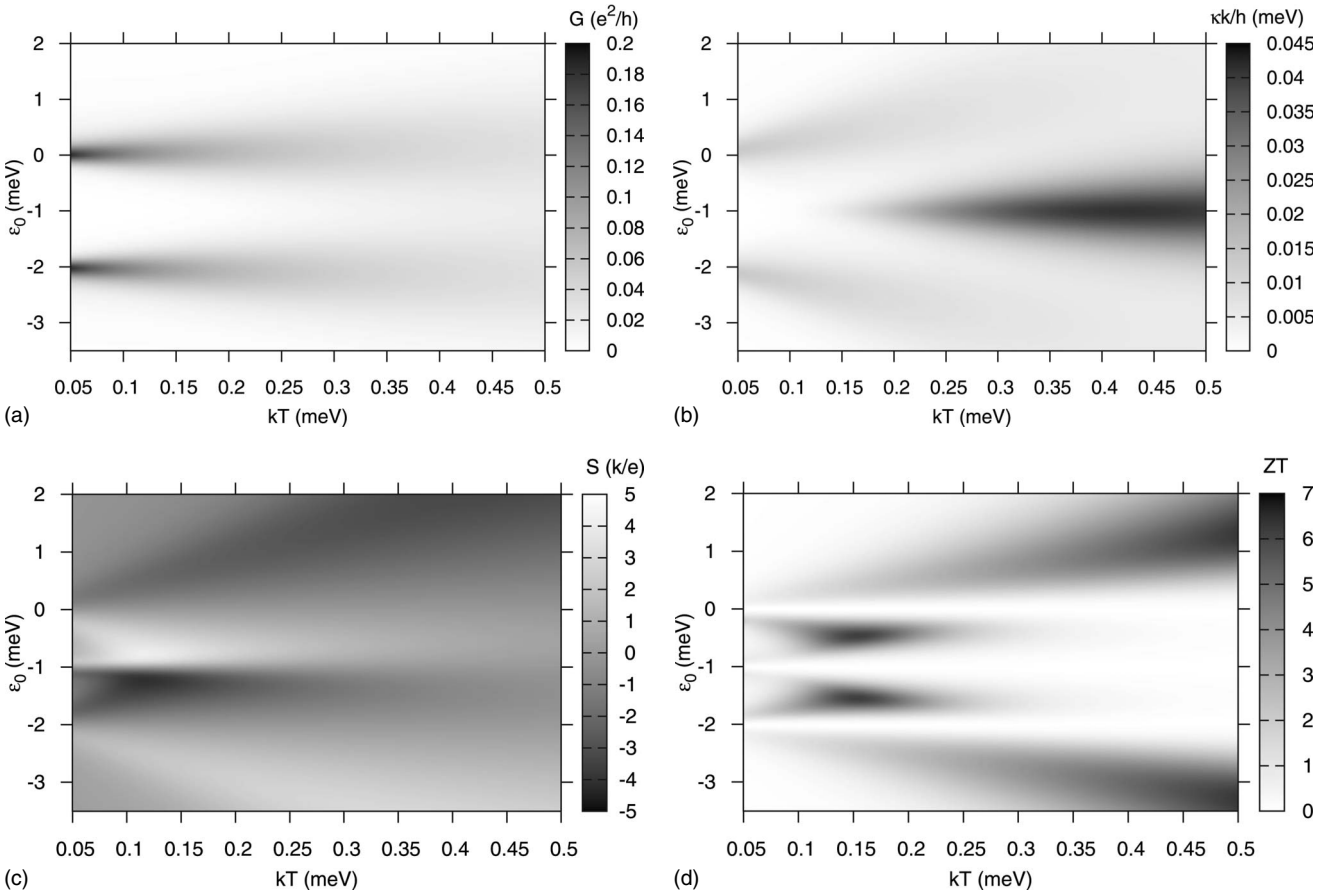

FIG. 1. (a) Linear electrical conductance G, (b) thermal conductance κ, (c) thermopower S, and (d) ZT as a function of level position and temperature, calculated for $\Gamma=0.1$ meV, $U=2$ meV, and $p=0.2$.

energy (the same for both electrodes) and p denotes the leads spin polarization.

To determine the transmission coefficient $\mathbf{T}(E)$, we use the nonequilibrium Green's function formalism based on the equation of motion method. Within the standard Hartree-Fock approximation, which is justified out of the Kondo regime, the energy-dependent Green's function, $G_{\sigma\sigma'}=\langle\langle d_\sigma, d^+_{\sigma'}\rangle\rangle$, satisfies the Dyson equation which can be written in matrix form as

$$(\mathbf{g}_0^{-1}-\mathbf{\Sigma})\mathbf{G}=\mathbf{I}, \tag{11}$$

where $g_{0\sigma\sigma'}=\delta_{\sigma\sigma'}(E-\varepsilon_0)^{-1}$ is the Green's function of the dot in the absence of both electron correlations and coupling to the leads, while $\mathbf{\Sigma}$ is the self-energy of the form

$$\mathbf{\Sigma}=\mathbf{g}_0^{-1}-(\mathbf{g}_U^{-1}-U\tilde{\mathbf{n}})^{-1}\mathbf{g}_U^{-1}\mathbf{g}_0^{-1}+\mathbf{\Sigma}_0 \tag{12}$$

with $g_{U\sigma\sigma'}=\delta_{\sigma\sigma'}(E-\varepsilon_0-U)^{-1}$, $\tilde{n}_{\sigma\sigma}=-n_{-\sigma}$, $\tilde{n}_{\sigma-\sigma}=n_{-\sigma\sigma}$, and $\mathbf{\Sigma}_0$ denoting the self-energy in the absence of Coulomb correlations. The occupation numbers $n_{\sigma\sigma'}=\langle d^+_\sigma d_{\sigma'}\rangle$ are expressed in terms of the lesser Green's functions as $n_{\sigma\sigma'}=-(i/2\pi)\int dE G^<_{\sigma'\sigma}$.

To find the lesser Green's function we use the Keldysh equation, $\mathbf{G}^<=\mathbf{G}^r\mathbf{\Sigma}^<\mathbf{G}^a$, with $\mathbf{\Sigma}^<$ determined according to the Ng ansatz;[39] $\mathbf{\Sigma}^<=\mathbf{\Sigma}_0^<(\mathbf{\Sigma}_0^r-\mathbf{\Sigma}_0^a)^{-1}(\mathbf{\Sigma}^r-\mathbf{\Sigma}^a)$, where $\mathbf{\Sigma}_0^<=-i(\mathbf{\Gamma}^L f_L+\mathbf{\Gamma}^R f_R)$ and $\mathbf{\Sigma}_0^r-\mathbf{\Sigma}_0^a=-i(\mathbf{\Gamma}^L+\mathbf{\Gamma}^R)$, whereas $\mathbf{\Sigma}^r-\mathbf{\Sigma}^a=-i\mathbf{\Gamma}^{eff}$, with $\mathbf{\Gamma}^{eff}$ calculated from Eq. (12). The transmission matrix $\mathbf{T}(E)$ is then given by the formula[40]

$$\mathbf{T}(E)=\frac{1}{2}(\mathbf{\Gamma}^L\mathbf{G}^r\tilde{\mathbf{\Gamma}}^R\mathbf{G}^a+\mathbf{\Gamma}^R\mathbf{G}^r\tilde{\mathbf{\Gamma}}^L\mathbf{G}^a), \tag{13}$$

where $\tilde{\mathbf{\Gamma}}^\beta=\mathbf{\Gamma}^\beta(\mathbf{\Gamma}^L+\mathbf{\Gamma}^R)^{-1}\mathbf{\Gamma}^{eff}$ and $\mathbf{G}^{r,a}$ are the retarded and advanced Green's functions calculated from the Dyson equation. When magnetic moments in both electrodes are collinear all matrices are diagonal, and $T_{\sigma\sigma'}(E)=\delta_{\sigma\sigma'}T_\sigma(E)$, with $T_\sigma(E)=\frac{\Gamma^L_\sigma\Gamma^R_\sigma}{\Gamma^L_\sigma+\Gamma^R_\sigma}i(G^r_{\sigma\sigma}-G^a_{\sigma\sigma})$ being the transmission coefficient in the spin channel σ.

IV. NUMERICAL RESULTS

Let us consider first the case when magnetic moments of the leads are aligned, i.e., the parallel (P) configuration ($\theta=0$). The electric conductance G, thermal conductance κ, thermopower S, and figure of merit ZT are shown in Fig. 1 as a function of temperature T and dot level position ε_0. The later can be tuned by external gate voltage, so the dependence on ε_0 is also referred to in the following as the gate voltage dependence. The calculations were performed for the spin polarization of leads corresponding to $p=0.2$. At relatively low temperatures, $kT\approx 0.5\Gamma$, the linear conductance G shows two sharp peaks corresponding to resonances when

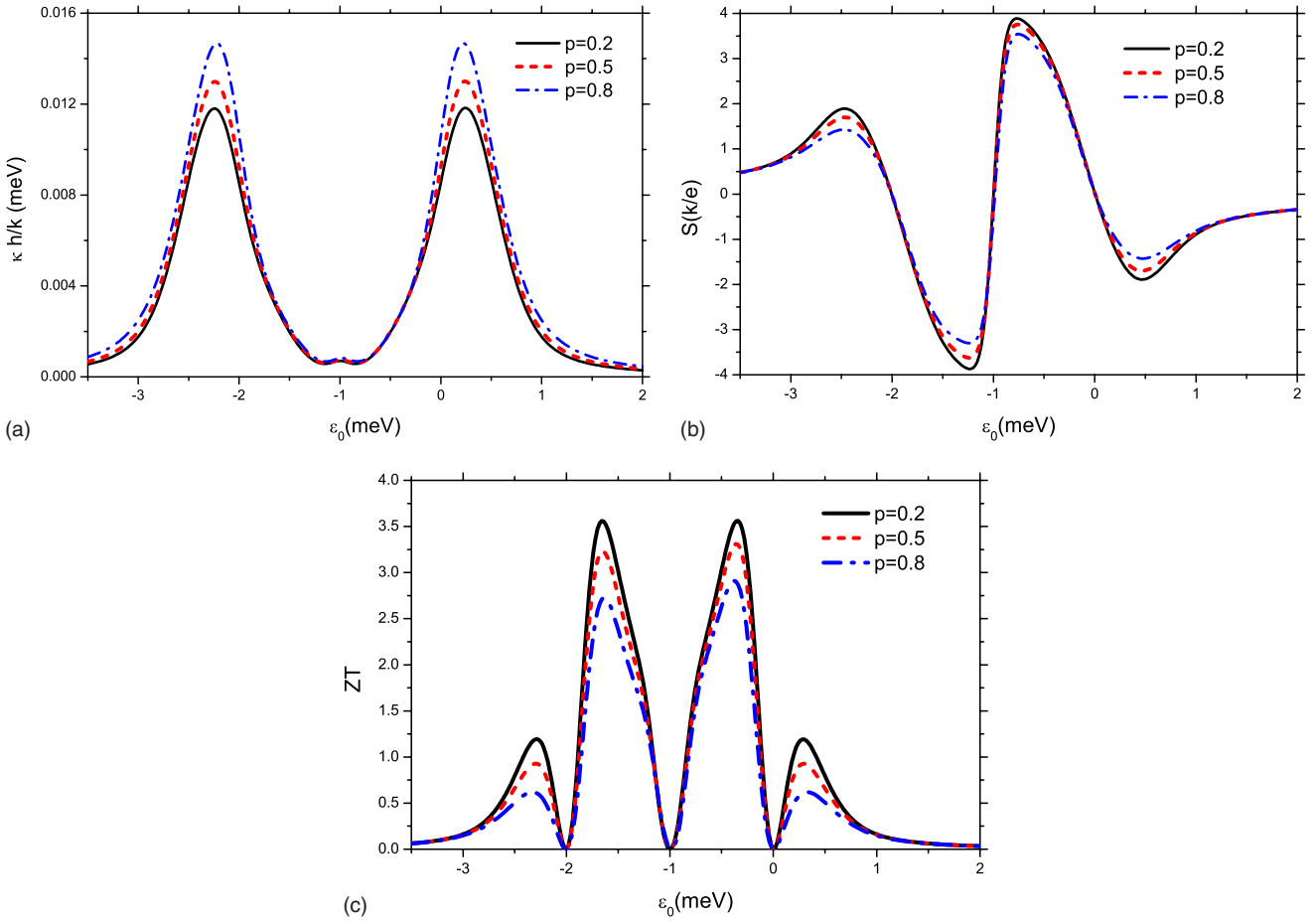

FIG. 2. (Color online) (a) Thermal conductance κ, (b) thermopower S, and (c) ZT as a function of the level position for indicated values of the spin polarization p. The other parameters are: $\Gamma=0.1$ meV, $U=2$ meV, and $kT=0.1$ meV.

either ε_0 or ε_0+U crosses the Fermi level in the leads ($\mu=0$), see Fig. 1(a). The Coulomb blockade region between the peaks is clearly visible. When temperature is increased, the peaks become wider and of lower intensity, while the Coulomb blockade effects are less pronounced. This behavior is well known and we show it only for comparison with the behavior of thermal conductance and thermopower.

The thermal conductance κ [Fig. 1(b)] at low temperatures also reveals two well-defined peaks, which roughly correspond to the peaks in the electrical conductance [Fig. 1(a)]. These peaks are explicitly shown in Fig. 2(a), where one of the curves (for $p=0.2$) corresponds to the cross-section of Fig. 1(b) at $kT=\Gamma=0.1$ meV. Two features of the spectra shown in Fig. 2(a) are worth mentioning. First, the peaks are slightly wider than the corresponding peaks in electrical conductance. Second, separation between the peaks is larger than the separation of electrical conductance peaks. Apart from this, behavior of κ with increasing temperature is different from that of G. The thermal conductance significantly increases with increasing T, and a broad maximum develops in the middle of the Coulomb blockade regime, which fully dominates the dependence of κ on the gate voltage. A precursor of this maximum is already seen at low temperatures in Fig. 2(a) as a very weak maximum in the middle of the Coulomb gap. The origin of this behavior can be accounted for as follows. Consider first the low-temperature regime. When ε_0 approaches the resonance from above, charge current starts to flow and a peak develops in charge conductance. Electron contribution to heat transfer is then mainly due to electrons resonantly tunneling through the system and heat conductance roughly follows the charge conductance. When ε_0 decreases further (e.g., due to gate voltage), the system goes to deep Coulomb blockade, where charge and heat conductances are suppressed, and then another resonance is reached when $\varepsilon_0=-U$. When temperature increases, the thermal distribution of electrons becomes broader. Owing to this distribution, tunneling electrons contribute differently to charge and heat conductances due to a different energy-dependent "weighting" (energy of a tunneling electron is irrelevant for charge current, but is essential for heat transfer). When ε_0 approaches the upper or lower resonance, this makes the peaks in heat conductance broader than in the charge conductance. When the system is in the symmetry point, $\varepsilon_0=-U/2$, charge current associated with electrons tunneling from the lead of higher temperature to that of lower temperature is compensated (in the absence of external voltage) by charge current associated with holes tunneling in the opposite directions. In turn, contributions from the holes and electrons to the heat conductance add then constructively, giving rise to the central peak visible in Fig. 1(b).

The corresponding behavior of the thermopower S with temperature and gate voltage [Fig. 1(c)] is less characteristic.

For kT on the order of Γ, thermopower S varies rather sharply in the vicinity of the symmetry point $\varepsilon_0=-U/2$, where S changes sign and reaches a sharp maximum on one side of the symmetry point and a minimum on the other side. Then S changes sign again when ε_0 further departs from the symmetry point. Such a dependence is consistent with other results obtained for QDs in the Coulomb blockade regime.[15,17,18] This behavior is also clearly shown in Fig. 2(b), where the curve corresponding to $p=0.2$ represents a cross-section of Fig. 1(c) at $kT=0.1$ meV. As the temperature is increased, the variation in S with gate voltage becomes smooth, and the maxima/minima become flat due to a relatively flat Fermi-Dirac distribution function.

Behavior of S with decreasing ε_0 [see Fig. 2(b)] can be understood as follows. As $\varepsilon_0>0$ and decreases approaching the resonance, electrons tunnel from the lead of higher temperature (left) to the lead of lower temperature (right), which gives rise to a voltage drop under the condition of the vanishing current. This voltage drop, and consequently the thermopower S, is positive (S in the units of k/e is negative due to negative electron charge). When ε_0 reaches the resonance, current due electrons tunneling from left to right is compensated by that due to tunneling of holes, and charge current vanishes at resonance. Accordingly, the thermopower also vanishes. When ε_0 is below the resonance, the net electron flow is then from right to left and S changes sign. The thermopower disappears and changes sign again for ε_0 in the middle of the Coulomb blockade regime from the reasons already discussed above. The situation in the second resonance, $\varepsilon_0=-U$, is similar to that for the upper one.

Figure of merit ZT is determined by the behavior of transport coefficients discussed above, i.e., of G, κ, and S. Accordingly, three narrow valleys can be seen in the gate voltage dependence of ZT [Figs. 1(d) and 2(c)]. These minima, with vanishing ZT, correspond to the points where $S=0$, i.e., to the resonances $\varepsilon_0=0$ and $-U$, and middle of the Coulomb gap $\varepsilon_0=-U/2$. This is explicitly shown in Fig. 2(c), where the curve for $p=0.2$ is a cross-section of Fig. 1(d) at $kT=0.1$ meV. The three minima as well as the appropriate four maxima are clearly seen. For $\Gamma\leq kT\leq 2\Gamma$, magnitude of ZT is considerably enhanced due to the Coulomb blockade effect, and one can expect strong thermoelectric efficiency in this region. The corresponding peaks in ZT are relatively narrow and high. For higher temperatures, however, the peaks become suppressed as the influence of Coulomb blockade on transport properties is then less important. The thermal conductance κ increases then considerably, reducing the tendency of the system toward thermoelectricity. Thus, the results clearly indicate on the role of Coulomb correlations in the charge- and heat-transport processes.

Variation in the main thermoelectric parameters, i.e., of the thermal conductance κ, thermopower S, and figure of merit ZT with the spin polarization of the leads is shown in Fig. 2 for $kT=\Gamma$. Basic features of the curves were discussed above. What is interesting to note is their relatively weak dependence on p, particularly in the case of thermopower S. Moreover, the thermal conductance increases with increasing spin polarization of the leads, while the absolute value of the thermopower S and the parameter ZT decrease with increasing polarization p. The increase in thermal conductance with increasing p is particularly pronounced at resonances, where the electrical conductance decreases with increasing p (not shown). This can be accounted for by taking into account that thermal conductance corresponds to the situation with zero-charge current. Thus, when increasing p one reduces electrical conductance and this way also the voltage required to block charge current, which in turn enhances thermal conductance. Behavior of the other parameters with p can be accounted for in a similar way.

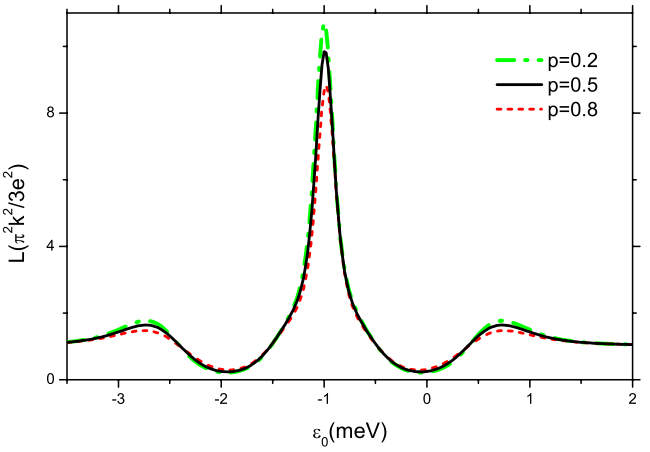

FIG. 3. (Color online) Lorentz ratio as a function of level position for indicated values of the spin polarization p. The other parameters are: $\Gamma=0.1$ meV, $U=2$ meV, and $kT=0.1$ meV.

Coulomb and quantum correlations in transport through nanoscopic systems usually lead to violation of the Wiedeman-Franz law. In Fig. 3 we show the Lorentz ratio, defined as $L=\kappa/GT$, measured in the units of $\pi^2k^2/3e^2$. Thus, the Lorenz ratio is also determined by the parameters discussed already above, i.e., G and κ. The Lorentz ratio strongly deviates from unity, indicating violation of the Wiedeman-Franz law, particularly in the Coulomb blockade regime. For the symmetry point, $\varepsilon_0=-U/2$, the ratio L is considerably enhanced by Coulomb blockade effect, and decreases with increasing polarization p. It is worth noting that this maximum in L corresponds to the central valley in the figure of merit. However, when ε_0 departs from $\varepsilon_0=-U/2$, the parameter L rapidly decreases. For $\varepsilon_0\gg 0$ and $\varepsilon_0\ll -U$, the Lorenz ratio L approaches the limit $L=1$. This is because transport in this regime is dominated by higher order tunneling (cotunneling) processes, which are not blocked by the Coulomb barrier. In the resonance region, the Lorenz ratio is reduced below the value of $L=1$, and increases with increasing p. The latter dependence is a consequence of a decrease in the electrical conductance and increase in thermal conductance [Fig. 2(a)] with increasing p, as discussed above.

The results presented up to now were for parallel alignment of the leads' magnetic moments. However, the thermoelectric properties and the corresponding quantities depend on relative alignment of the magnetic moments, and this dependence may be quite pronounced when spin polarization of the leads is large. In an ideal case one could assume perfect spin polarization for the leads, like in some half-metallic ferromagnets (with $|p|\approx 1$). Therefore, in the following calculations we assumed $p=0.95$. Variation in the thermal con-

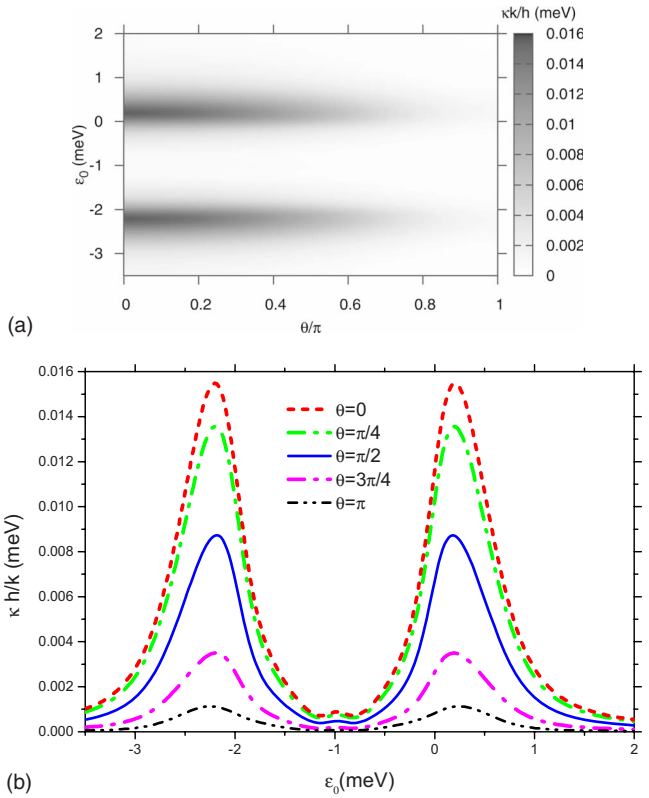

FIG. 4. (Color online) Thermal conductance κ (a) as a function of the level position ε_0 and angle θ and (b) as a function of ε_0 for indicated values of θ. The other parameters are: $p=0.95$, $\Gamma=0.1$ meV, $U=2$ meV, and $kT=0.1$ meV.

ductance κ with the angle θ between magnetic moments and position of the dot level is shown in Fig. 4(a). Several cross-sections of this figure for specific values of the angle θ are shown in Fig. 4(b). The thermal conductance decreases monotonically with increasing θ and is relatively low in the antiparallel (AP) configuration. This behavior resembles that of electrical conductance (not shown). In the parallel configuration transport takes place between spin-majority electron bands in both leads or spin-minority bands in both leads. The situation changes when the configuration of magnetic moments is varied from parallel to antiparallel. Then, electrons of both spin-orientations tunnel between spin-majority and spin-minority bands, and the total conductance (and also thermal conductance) is suppressed in comparison to that in the parallel configuration.

Gate voltage dependence of the thermopower S is shown in Fig. 5(a) for different values of the angle between magnetic moments. Now the dependence on the angle θ is less pronounced. Since the thermopower depends on relative orientation of the electrodes' magnetic moments, one can define magnetothermopower (MTP), $\mathrm{MTP}=[S(0)-S(\pi)]/S(\pi)$, with $S(0)$ and $S(\pi)$ denoting thermopower in the P and AP configurations, respectively.[35] Gate voltage dependence of MTP, corresponding to Fig. 5(a), is presented in Fig. 5(b). The magnetothermopower reveals resonancelike nature at the points $\varepsilon_0=0$, $-U/2$, and $-U$, i.e., at the points where S vanishes. The angular variation in the magnetothermopower, defined by the formula $\mathrm{MTP}(\theta)=[S(0)-S(\theta)]/S(\theta)$, is shown in Fig. 5(c). MTP is generally negative, i.e., thermopower increases when configuration is varied from parallel to antiparallel. However, small positive MTP can occur in a certain range of the angle θ and level energy ε_0. We recall that thermopower vanishes at resonances and also in the middle of the Coulomb blockade area. Accordingly, the MTP has singularities at these points, as show in Fig. 5(b). Thus, when ε_0 is close to resonance, both $S(0)$ and $S(\theta)$ are also small and a nonmonotonic angular dependence of electron tunneling may lead to the corresponding nonmonotonic angular variation in MTP.

The corresponding angular variation in the Lorenz ratio L and figure of merit ZT is shown in Figs. 6(a) and 6(b), respectively. This dependence is rather weak, particularly in the case of the Lorenz ratio, where the most pronounced dependence on the angle between magnetic moments of the leads appears in the symmetrical situation, $\varepsilon_0=-U/2$, where L is significantly enhanced. The values of ZT also monotonically increase with increasing θ and the highest values can be observed in the antiparallel configuration. Results presented in Fig. 6(b) confirm the conclusion that Coulomb blockade effects strongly influence thermoelectric efficiency.

V. SPIN THERMOELECTRIC EFFECTS

When spin accumulation in the external leads becomes relevant, e.g., due to long spin relaxation time, the voltage probe can measure chemical potentials at distances from the interface between the lead and dot, which is smaller than the spin-diffusion length. In such a case we have to take into account the spin splitting of the chemical potential in the leads. This makes the situation more complex and physically richer than that described above. Therefore, for clarity reasons we assume in this section a collinear magnetic configuration, for which the transmission matrix $\mathbf{T}(E)$ is diagonal, and therefore L_n can be written as $L_n=\Sigma_\sigma L_{n\sigma}$. Apart from this, in addition to the above used charge bias ΔV one can introduce spin bias ΔV_{spin} according the formula

$$\Delta V_\sigma = \Delta V + \hat{\sigma}\Delta V_{spin}, \tag{14}$$

where ΔV_σ is given by the difference in chemical potentials of the two leads in the spin channel σ, while $\hat{\sigma}=\pm 1$ for $\sigma=\uparrow$ (upper sign) and $\sigma=\downarrow$ (lower sign). From the above follows that spin bias appears when there is a spin accumulation, while $\Delta V_{spin}=0$ in the absence of spin accumulation.

The definition of thermopower in Sec. II was based on the assumption of vanishing charge current. Since the two spin channels are independent and the transmission coefficient depends on electron spin, the condition $I=I_\uparrow+I_\downarrow=0$ is then associated with a nonzero spin current, $I_{spin}=(\hbar/2e)(I_\uparrow-I_\downarrow)\neq 0$. When spin accumulation is present, one can define thermopower calculated on the condition of vanishing simultaneously both spin current and charge current, or equivalently on the condition of vanishing charge current I_σ in each spin channel.

Equations (1) and (2) can be then rewritten as

$$I_\sigma = eL_{0\sigma}\Delta\mu_\sigma + \frac{e}{T}L_{1\sigma}\Delta T \tag{15}$$

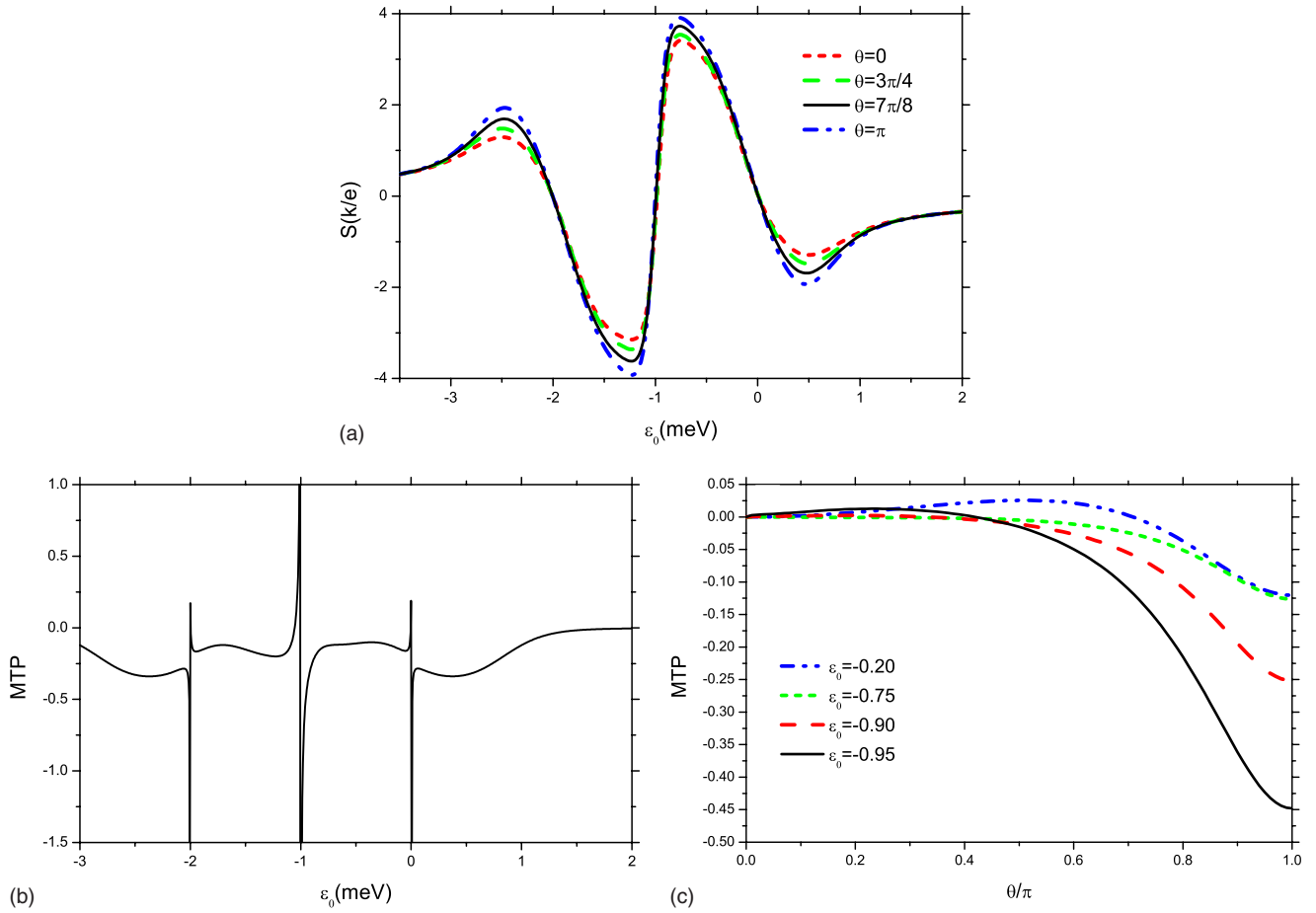

FIG. 5. (Color online) (a) Thermopower for indicated values of θ and (b) magnetothermopower as a function of the level position. MTP (θ) for indicated values of ε_0 (c). The other parameters are: $p=0.95$, $\Gamma=0.1$ meV, $U=2$ meV, and $kT=0.1$ meV.

for charge current in the spin channel σ, and

$$I_Q = -\sum_\sigma \left(L_{1\sigma}\Delta\mu_\sigma + \frac{1}{T}L_{2\sigma}\Delta T \right) \tag{16}$$

for the heat current.

The spin and charge currents can be written as[41]

$$I = G\Delta V + G^m \Delta V_{spin}, \tag{17}$$

$$I_{spin} = G_{spin}\Delta V + G^m_{spin}\Delta V_{spin} \equiv \frac{\hbar}{2e}(G^m \Delta V + G\Delta V_{spin}) \tag{18}$$

with

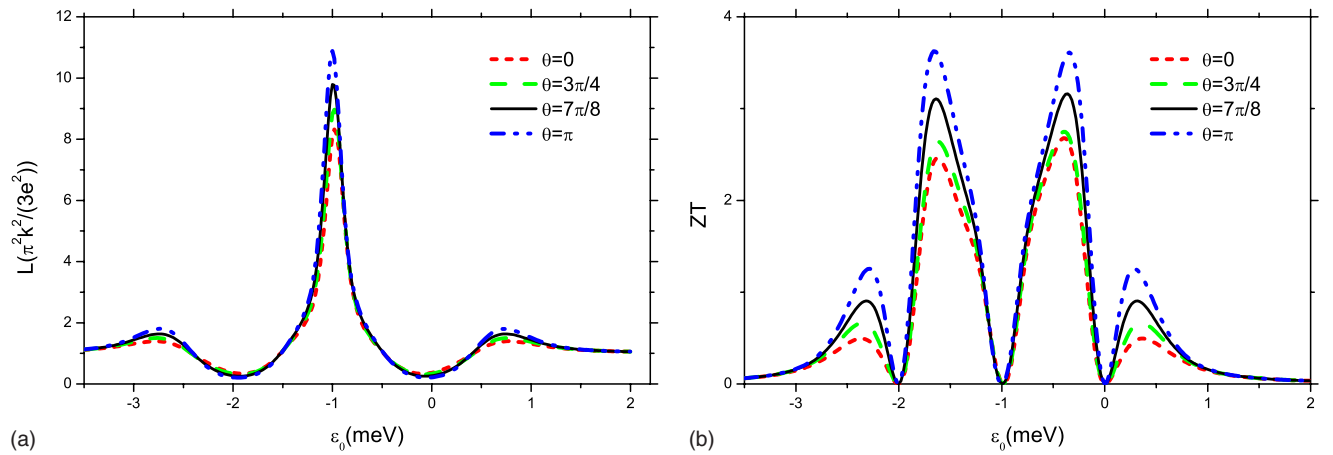

FIG. 6. (Color online) (a) Lorentz ratio and (b) ZT as a function of the level position for indicated values of θ. The other parameters are: $p=0.95$, $\Gamma=0.1$ meV, $U=2$ meV, and $kT=0.1$ meV.

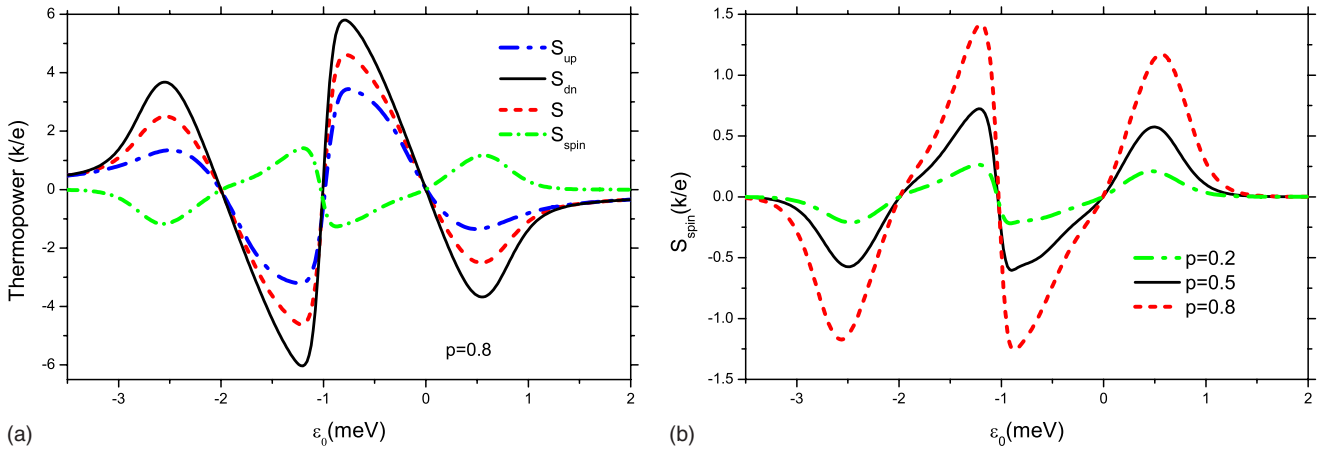

FIG. 7. (Color online) Thermopower as a function of level position calculated under the condition of $I_\sigma=0$ for indicated spin polarization of the leads. The other parameters are: $\Gamma=0.1$ meV, $U=2$ meV, and $kT=0.1$ meV.

$$G = G_\uparrow + G_\downarrow = e^2(L_{0\uparrow} + L_{0\downarrow}), \tag{19}$$

$$G^m = e^2(L_{0\uparrow} - L_{0\downarrow}). \tag{20}$$

In turn, the heat conductance is given by

$$\kappa = \sum_\sigma \kappa_\sigma = \sum_\sigma \frac{1}{T}\left(L_{2\sigma} - \frac{L_{1\sigma}^2}{L_{0\sigma}}\right). \tag{21}$$

It is thus reasonable to introduce the spin-dependent thermopower,

$$S_\sigma = \Delta V_\sigma/\Delta T = -L_{1\sigma}/eTL_{0\sigma}, \tag{22}$$

determined on the condition that electric current in the channel σ is equal to zero, $I_\sigma=0$. Accordingly, ΔV_σ corresponds to the spin-dependent thermoelectric voltage, which can be rewritten in the form of Eq. (14), with $\Delta V=(\Delta V_\uparrow+\Delta V_\downarrow)/2$ denoting the thermally induced charge voltage, and $\Delta V_{spin}=(\Delta V_\uparrow-\Delta V_\downarrow)/2$ being the corresponding spin voltage. Following this, one can introduce spin thermopower S_{spin} in addition to the charge thermopower S,

$$S_{spin} = \frac{\Delta V_{spin}}{\Delta T} = \frac{1}{2}(S_\uparrow - S_\downarrow) = -\frac{1}{2eT}\left(\frac{L_{1\uparrow}}{L_{0\uparrow}} - \frac{L_{1\downarrow}}{L_{0\downarrow}}\right), \tag{23}$$

$$S = \frac{\Delta V}{\Delta T} = \frac{1}{2}(S_\uparrow + S_\downarrow) = -\frac{1}{2eT}\left(\frac{L_{1\uparrow}}{L_{0\uparrow}} + \frac{L_{1\downarrow}}{L_{0\downarrow}}\right). \tag{24}$$

Spin-dependent thermopower S_σ is presented in Fig. 7(a), where we also show the thermopower S and spin thermopower S_{spin}. In general, the curves representing $S_\uparrow$ and $S_\downarrow$, as well as S, are similar to the ones found from the condition $I=0$. The spin thermopower, in turn, strongly varies with the spin polarization of electrodes and increases with p, as illustrated in Fig. 7(b). Moreover, the sign of spin thermopower is opposite to the sign of charge thermopower as voltage induced in the channel corresponding to minority spins is higher. It is worth noting that both charge and spin thermopower disappear at resonances as well as in the middle of the Coulomb gap. Note, that we assumed the temperature drop independent of spin. In a more general situation, however, the spin-dependent temperature can be included as well.

Figure of merit ZT, defined by the formula (7) and calculated in the situation when currents in both spin channels are equal to zero, is presented in Fig. 8(a). Now, the magnitude of ZT increases with p in the Coulomb blockade region, and the valley between the two main peaks becomes narrower for higher p. This corresponds to the strong increase in thermopower efficiency in the minority spin channel. We also note, that one can introduce a spin analog of the figure of merit ZT given by Eq. (7), i.e.,

$$Z_{spin}T = \frac{(2e/\hbar)G_{spin}S_{spin}^2 T}{\kappa}, \tag{25}$$

where G_{spin} is defined in Eq. (18), while κ and S_{spin} are given by Eqs. (21) and (23), respectively. Variation in $Z_{spin}T$ with the level position is shown in Fig. 8(b).

VI. NONLINEAR THERMOPOWER

Assume now the situation when the temperature difference between the two leads is large enough, so the linear description ceases to be valid. Consider first the case of vanishing spin accumulation (zero spin voltage). Differential thermopower, defined as $S_{diff}=dV/dT$, is presented in Fig. 9(a) for $p=0.9$ and parallel configuration of magnetic moments. Temperature of the right electrode is assumed constant, $kT_R=\Gamma$, while temperature of the left electrode is higher by $k\Delta T_L$. The voltage V between two electrodes is generated by the temperature difference under the condition of vanishing charge current, $I=0$. In nonlinear situation the current is calculated according to the formula given by Meir:[42] $I=\frac{e}{h}\Sigma_\sigma\int dE T_\sigma(E)[f_L(E)-f_R(E)]$ with $f_{L(R)}$ denoting the Fermi-Dirac distribution function in the left (right) electrode. For the chosen energy level, $\varepsilon_0=-1.65$ meV, S_{diff} is negative and changes in a monotonic way; its absolute magnitude decreases with increasing ΔT_L and is practically equal to zero for $k\Delta T_L > 5\Gamma$. This result is consistent with the one presented in Fig. 1 for the linear response regime, as the thermoelectric efficiency is low at higher temperatures due to weak influence of Coulomb blockade.

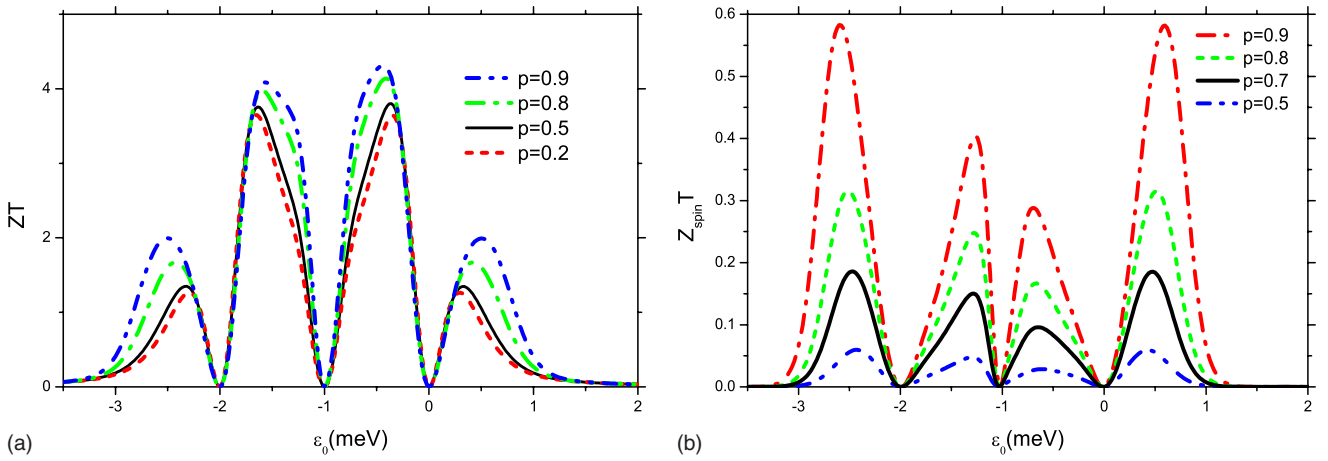

FIG. 8. (Color online) (a) Figure of merit ZT and (b) $Z_{spin}T$ as a function of level position calculated under the condition of $I_\sigma=0$ for indicated values of p. The other parameters are: $\Gamma=0.1$ meV, $U=2$ meV, and $kT=0.1$ meV.

When spin accumulation is relevant, to compensate the current in each spin channel one has to apply spin-dependent voltage (spin and charge biases). The corresponding spin-dependent differential thermopower, defined as $S^\sigma_{diff}=dV_\sigma/dT$, is presented in Fig. 9(b) for both spin channels and for $p=0.9$. Functional dependence of S^σ_{diff} is similar to S_{diff}, but at small values of $k\Delta T_L$ the thermopower strongly depends on the spin orientation and reaches the largest absolute values for minority spins. Spin and charge thermopower, defined as $S_{diff}=(1/2)(S^\uparrow_{diff}+S^\downarrow_{diff})=dV/dT$ and $S^{spin}_{diff}=(1/2)(S^\uparrow_{diff}-S^\downarrow_{diff})=dV_{spin}/dT$ are also shown there.

VII. SUMMARY AND DISCUSSION

We have considered thermoelectric coefficients in the Coulomb blockade regime for a QD attached to ferromagnetic electrodes. The considerations reveal a significant role of the blockade effect in charge and heat transport processes, which manifests in a substantial increase in thermoelectric efficiency described quantitatively by the dimensionless figure of merit. For gate voltages corresponding to the Coulomb blockade region, ZT shows two peaks with intensities strongly dependent on temperature, leads' polarization p, and magnetic configuration of the system. The blockade effects become less significant with increasing temperature, so the intensities of peaks in ZT are lower. Magnitude of ZT also diminishes in systems with strongly polarized electrodes and for parallel configuration of the system, as the Coulomb blockade is partially reduced in majority spin channel due to strong coupling with the leads. When configuration of magnetic moments is varied from parallel to antiparallel, the Coulomb blockade effects become important for both spin channels which leads to gradual increase in ZT. At a given temperature, the peaks in ZT achieve maximal intensities when both spin channels are fully equivalent, which takes place for antiparallel configuration in symmetric system or for nonmagnetic case. In such a situation the charge current

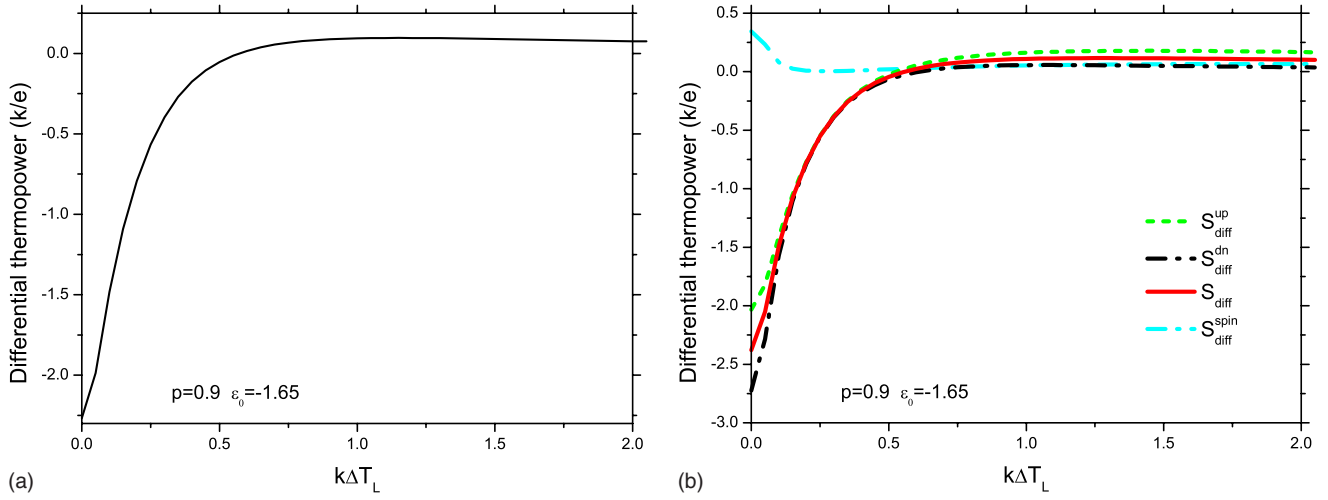

FIG. 9. (Color online) Differential thermopower (a) in the absence of spin accumulation and (b) with spin accumulation as a function of temperature difference for indicated level position and polarization p, calculated for the condition of (a) vanishing charge current and (b) spin and charge currents, $\Gamma=0.1$ meV, $U=2$ meV, and $kT_R=0.1$ meV.

$I=I_{\uparrow}+I_{\downarrow}$ as well as the spin current $I_s=(\hbar/2e)(I_{\uparrow}-I_{\downarrow})$ vanish simultaneously.

The spin Seebeck effect has been observed recently by Uchida *et al.*[31] in a ferromagnetic transition-metal slab. One also may expect that similar effects can be observable in spin valves based on quantum dots, like those discussed in this manuscript, particularly when half-metallic ferromagnets will be used. Moreover, the experiment may turn out much simpler when the concept of spin battery will be realized practically.

ACKNOWLEDGMENTS

This work was supported by funds of the Polish Ministry of Science and Higher Education through National Scientific network ARTMAG.

[1] P. Reddy, S. Y. Jang, R. A. Segalman, and A. Majumdar, Science **315**, 1568 (2007).
[2] A. I. Hochbaum, R. Chen, R. D. Delgado, W. Liang, E. C. Garnett, M. Najarian, A. Majumdar, and P. Yang, Nature (London) **451**, 163 (2008).
[3] K. Baheti, J. A. Malen, P. Doak, P. Reddy, S. Y. Jang, T. D. Tilley, A. Majumdar, and R. A. Segalman, Nano Lett. **8**, 715 (2008).
[4] A. I. Boukai, Y. Bunimovich, J. Tahir-Kheli, J. K. Yu, W. A. Goddard III, and J. R. Heath, Nature (London) **451**, 168 (2008).
[5] K. Schwab, E. A. Henriksen, J. M. Worlock, and M. L. Roukes, Nature (London) **404**, 974 (2000).
[6] L. G. C. Rego and G. Kirczenow, Phys. Rev. Lett. **81**, 232 (1998).
[7] Y. Dubi and M. Di Ventra, Nano Lett. **9**, 97 (2009).
[8] T. Markussen, A. P. Jauho, and M. Brandbyge, Phys. Rev. B **79**, 035415 (2009).
[9] M. Galperin, A. Nitzan, and M. A. Ratner, Mol. Phys. **106**, 397 (2008).
[10] A. M. Lunde, K. Flensberg, and L. I. Glazman, Phys. Rev. Lett. **97**, 256802 (2006).
[11] D. Segal, Phys. Rev. B **72**, 165426 (2005).
[12] F. Pauly, J. K. Viljas, and J. C. Cuevas, Phys. Rev. B **78**, 035315 (2008).
[13] B. Wang, Y. Xing, L. Wan, Y. Wei, and J. Wang, Phys. Rev. B **71**, 233406 (2005).
[14] Y. S. Liu, Y. R. Chen, and Y. C. Chen, arXiv:0902.3876 (unpublished).
[15] C. W. J. Beenakker and A. A. M. Staring, Phys. Rev. B **46**, 9667 (1992).
[16] Y. M. Blanter, C. Bruder, R. Fazio, and H. Schoeller, Phys. Rev. B **55**, 4069 (1997).
[17] M. Turek and K. A. Matveev, Phys. Rev. B **65**, 115332 (2002).
[18] J. Koch, F. von Oppen, Y. Oreg, and E. Sela, Phys. Rev. B **70**, 195107 (2004).
[19] B. Kubala and J. Konig, Phys. Rev. B **73**, 195316 (2006).
[20] B. Kubala, J. Konig, and J. Pekola, Phys. Rev. Lett. **100**, 066801 (2008).
[21] X. Zianni, Phys. Rev. B **75**, 045344 (2007).
[22] D. Boese and R. Fazio, Europhys. Lett. **56**, 576 (2001).
[23] B. Dong and X. L. Lei, J. Phys.: Condens. Matter **14**, 11747 (2002).
[24] M. Krawiec and K. I. Wysokinski, Phys. Rev. B **73**, 075307 (2006).
[25] R. Sakano, T. Kita, and N. Kawakami, J. Phys. Soc. Jpn. **76**, 074709 (2007).
[26] R. Scheibner, H. Buchmann, D. Reuter, M. N. Kiselev, and L. W. Molenkamp, Phys. Rev. Lett. **95**, 176602 (2005).
[27] M. Yoshida and L. N. Oliveira, Physica B **404**, 3312 (2009).
[28] M. Tsaousidou and G. P. Triberis, *Physics of Semiconductors: 28th International Conference on the Physics of Semiconductors ICPS 2006*, AIP Conf. Proc. Vol. 893 (AIP, New York, 2007), p. 801.
[29] P. Murphy, S. Mukerjee, and J. Moore, Phys. Rev. B **78**, 161406(R) 2008.
[30] C. M. Finch, V. M. Garcia-Suarez, and C. J. Lambert, Phys. Rev. B **79**, 033405 (2009).
[31] K. Uchida, S. Takahashi, K. Harii, J. Ieda, W. Koshibae, K. Ando, S. Maekawa, and E. Saitoh, Nature (London) **455**, 778 (2008).
[32] L. Gravier, S. Serrano-Guisan, F. Reuse, and J. P. Ansermet, Phys. Rev. B **73**, 024419 (2006); **73**, 052410 (2006).
[33] S. Serrano-Guisan, G. di Domenicantonio, M. Abid, J. P. Abid, M. Hillenkamp, L. Gravier, J. P. Ansermet, and C. Felix, Nature Mater. **5**, 730 (2006).
[34] O. Tsyplyatyev, O. Koshuba, and V. I. Fal'ko, Phys. Rev. B **74**, 132403 (2006).
[35] M. Hatami, G. E. W. Bauer, Q. Zhang, and P. J. Kelly, Phys. Rev. B **79**, 174426 (2009).
[36] Y. Dubi and M. Di Ventra, Phys. Rev. B **79**, 081302 (2009).
[37] C. D. Mahan, *Many-Particle Physics* (Plenum, New York, 2000).
[38] W. Rudzinski, J. Barnas, R. Swirkowicz, and M. Wilczynski, Phys. Rev. B **71**, 205307 (2005).
[39] T. K. Ng, Phys. Rev. Lett. **68**, 1018 (1992); **70**, 3635 (1993).
[40] R. Swirkowicz, M. Wilczynski, M. Wawrzyniak, and J. Barnas, Phys. Rev. B **73**, 193312 (2006).
[41] R. Swirkowicz, J. Barnas, and M. Wilczynski, J. Magn. Magn. Mater. **321**, 2414 (2009).
[42] Y. Meir, N. S. Wingreen, and P. A. Lee, Phys. Rev. Lett. **70**, 2601 (1993).